Metamorphic and Lattice-Matched GaInP Rear-Heterojunction Solar Cells for Improved Performance at Elevated Temperatures

Mijung Kim, Yukun Sun, and Minjoo Larry Lee

***Abstract*—We present the characteristics of *n*-on-*p* front-junction (FJ) and rear-heterojunction (RHJ) GaInP solar cells at operating temperatures (*T*) up to 300 °C. Photovoltaic cells with efficient operation at high *T* may be important for satellite missions near the sun or as laser power converters for sensors operating in harsh environments. In this article, we show that the time-resolved photoluminescence lifetime (τ_{TRPL}) values in both lattice-matched (LM) *n*-$Ga_{0.51}In_{0.49}P$ and metamorphic (MM) *n*-$Ga_{0.37}In_{0.63}P$ double heterostructures are high and increase significantly with *T*. In contrast, the τ_{TRPL} values in their *p*-type counterparts are lower and decrease with *T*. We go on to demonstrate both LM and MM solar cells in FJ and RHJ configurations. The internal quantum efficiency (IQE) of MM RHJ cells increases significantly up to $T = 300$ °C due to the increase in both τ_{TRPL} and the linear increase in diffusivity with *T*. In contrast, the IQE for MM FJ cells is nearly unchanged as *T* increases, while the IQE of LM cells drops sharply across all wavelengths. RHJ cells maintain higher open-circuit voltage and fill factor than their FJ counterparts, leading to a significant efficiency advantage at $T = 100$–300 °C. Taken together, our work shows that MM cells perform well at elevated *T* and that RHJ cells are promising for high-*T* operation.**

***Index Terms*—High-temperature photovoltaics, metamorphic (MM) GaInP, rear-heterojunction (RHJ).**

I. Introduction

PHOTOVOLTAIC devices with efficient operation at high temperatures (*T*) may be a crucial component for challenging space applications, such as near-sun satellites and Venus missions [1], [2], [3]. They can also serve as a power source for sensors and electronics in aerospace and automotive applications, as well as in harsh environments, such as gas turbines and geothermal wells [4], [5], [6], [7]. Previous studies showed that lattice-matched (LM) III–V front-junction (FJ) solar cells can achieve reasonable performance even at temperatures as high as 400 °C [1], [8], [9].

An unavoidable factor for photovoltaic devices operating at high *T* is the exponential increase in intrinsic carrier concentration (n_i) and, hence, dark current as *T* increases, leading to strong decrement in both open-circuit voltage (V_{OC}) and fill factor (FF). Despite a slight increase in short-circuit current density (J_{SC}) due to the decrease in bandgap energy (E_g), the overall efficiency undergoes significant degradation at high *T* [1], [10], [11].

Another effect at elevated *T* is that a greater proportion of charge carriers can attain enough energy to surmount heterojunction barriers (e.g., the window and back surface field or BSF layers), leading to increased recombination at the free surface and further increased dark current [12]. The rate of thermionic emission decreases exponentially with effective barrier height [13], and previous work revealed that the performance of LM $Ga_{0.51}In_{0.49}P$ solar cells at high *T* improved with increasing E_g of the LM $(Al_xGa_{1-x})_{0.51}In_{0.49}P$ passivation layer due to the higher barrier [12]. However, further reduction of thermionic emission for LM GaInP cells is challenging due to material limitations that restrict the E_g of the LM III–V cladding layer to ≤ 2.3 eV (LM $Al_{0.52}In_{0.48}P$).

The need to suppress thermionic emission motivates the investigation of metamorphic (MM) $Ga_{0.37}In_{0.63}P$ for high-*T* applications. At room temperature (RT), E_g of MM $Ga_{0.37}In_{0.63}P$ and LM $Ga_{0.51}In_{0.49}P$ are 1.7 eV and 1.9 eV, respectively, while E_g of MM $Al_{0.38}In_{0.62}P$ and LM $Al_{0.52}In_{0.48}P$ window layers are $\sim$2.3 eV in both cases. The larger ΔE_g in the MM cells translates to higher barrier heights than in LM cells and an exponential suppression in thermionic emission.

Another potential approach to achieve improved performance at elevated *T* is employing a rear-heterojunction (RHJ) configuration. Under standard conditions, RHJ cells can have a lower dark current and higher V_{OC} than their FJ counterparts [14], [15], [16] due to the reduction of trap-assisted recombination in the space charge region. Moreover, the valence bands in phosphides have a significantly higher density of states than their corresponding conduction bands [17], [18], resulting in reduced thermal spreading of minority holes compared with electrons; i.e., at a given *T*, minority holes tend to occupy states close to the valence band edge. RHJ cells only collect minority holes [14] and may, therefore, exhibit lower thermionic emission loss compared with FJ cells.

Manuscript received 14 November 2023; revised 14 February 2024; accepted 25 March 2024. This work was supported by the NSF under Grant 1810265. The work of Yukun Sun was supported by the NSF under Grant 1736181 and Grant 1810265. *(Corresponding author: Minjoo Larry Lee.)*

Mijung Kim and Minjoo Larry Lee are with the Department of Electrical and Computer Engineering, University of Illinois Urbana-Champaign, Urbana, IL 61801 USA, and also with the Nick Holonyak, Jr. Micro and Nanotechnology Laboratory, University of Illinois Urbana-Champaign, Urbana, IL 61801 USA (e-mail: mijungk2@illinois.edu; mllee@illinois.edu).

Yukun Sun was with the Department of Electrical Engineering, Yale University, New Haven, CT 06520 USA, and also with the Nick Holonyak, Jr. Micro and Nanotechnology Laboratory, University of Illinois Urbana-Champaign, Urbana, IL 61801 USA. He is now with the KLA-Tencor, Ann Arbor, MI 48105 USA (e-mail: yukun.sun@kla-tencor.com).

Color versions of one or more figures in this article are available at https://doi.org/10.1109/JPHOTOV.2024.3384916.

Digital Object Identifier 10.1109/JPHOTOV.2024.3384916

In this article, we compare the performance of FJ and RHJ cells at elevated T for both LM and MM GaInP. We demonstrate that the quantum efficiency (QE) of LM FJ cells decreases significantly with T, while MM cells maintain similar QE at high T due to longer lifetimes and higher barrier heights. In contrast, QE of LM and MM RHJ cells increase with T, in agreement with our observation of increasing minority hole lifetime with T. Next, we show that the dark current advantage of RHJ cells is maintained as T increases, leading to higher V_{OC}, FF, and efficiency than FJ cells at $T = 100$–300 °C. These results show that RHJ cells are promising for high-T applications and that MM materials with large heterojunction band offsets are helpful in suppressing thermionic emission.

II. Experimental Methods

All solar cells and double heterostructures (DHs) in this work were grown using a Veeco Mod Gen-II solid-source molecular beam epitaxy system and annealed using an AllWin rapid thermal annealing (RTA) system. RTA processes were carried out under N_2 ambient with a ramp rate of 20 °C/s. The optimal RTA conditions (850–1000 °C, 1–30 s) for DHs and solar cells were chosen based on maximizing the steady-state photoluminescence intensity [19]. In our previous studies, these cells showed comparable performance to metalorganic vapour-phase epitaxy (MOVPE)-grown cells [15], [19].

The DHs, consisting of a 500 nm GaInP active layer with RT E_g of either 1.7 eV (MM) or 1.9 eV (LM), were grown at a substrate temperature of 460 °C and growth rate of 0.5 μm/hr for time-resolved photoluminescence (TRPL) studies. GaInP active layers were lightly doped with electron (hole) concentrations of n_o (p_o) $= 1.0 \times 10^{17}$ cm^{-3}; 100 nm n-InAlP (p-AlGaInP) barriers were doped with n_o (p_o) $= 1.0\times10^{18}$ cm^{-3}. The details about the DHs are described in previous papers [19], [20].

The growth structures of MM 1.7 eV and LM 1.9 eV GaInP FJ and RHJ solar cells are illustrated in Fig. 1(a)–(d). To ensure fair comparisons, similar layer structures were implemented for both MM and LM devices. The FJ cells comprise a 100 nm MM 2.0 eV p-$Al_{0.19}Ga_{0.19}In_{0.62}P$ (LM 2.2 eV p-$Al_{0.24}Ga_{0.28}In_{0.48}P$) BSF, 50 nm MM or LM p-GaInP with graded doping, 690 nm p-GaInP base, 70 nm n-GaInP emitter, 20 nm MM or LM n-AlInP window, and 200 nm MM n-InGaAs (n-GaAs) contact. The RHJ cells consist of a 100 nm MM 2.0 eV p-AlGaInP (LM 2.2 eV p-AlGaInP) BSF, 810 nm MM or LM n-GaInP emitter, 20 nm MM or LM n-AlInP window, and 200 nm n-InGaAs (n-GaAs) contact. A bridge layer ($p_o = 2.0\times10^{18}$ cm^{-3}) in MM cells consisting of 50 nm 2.0 eV p-AlGaInP and 50 nm p-GaInP between the heavily p-doped buffer ($p_o = 4.0\times10^{18}$ cm^{-3}) and the lightly p-doped BSF ($p_o = 1.0 \times 10^{17}$ cm^{-3}) was introduced to avoid majority hole blocking. In a previous report, we showed a low threading dislocation density of 6–7 $\times$ 10^5 cm^{-2} in MM $Ga_{0.37}In_{0.63}P$ solar cells [19]. Solar cells were fabricated similar to our previous works [21], [22] with Ti/Au and Cr/Au for front and back metal contacts. No antireflection coatings were applied.

All T-dependent measurements were performed using a variable T Linkam stage (HFS600E-PB4) with a temperature controller (T95-PE). TRPL measurements were conducted under low-level injection conditions using time-correlated single-photon counting and a 532 nm pulsed laser with a 1 mm diameter spot size, 2.5 mW average power, 6 ps pulse width, and 3.6 MHz repetition rate. Lighted current–voltage (LIV) measurements were conducted under approximate AM1.5G illumination with an ABET Technologies 10500 solar simulator to determine V_{OC}, bandgap-voltage offset ($W_{OC} = E_g/q - V_{OC}$), J_{SC}, FF, and efficiency (η). External quantum efficiency (EQE) and specular reflectance (R) were measured using a PV measurements QEX7 system; internal quantum efficiency (IQE) was estimated as IQE $=$ EQE/(1$-R$). Band diagrams were simulated using BandProf software.

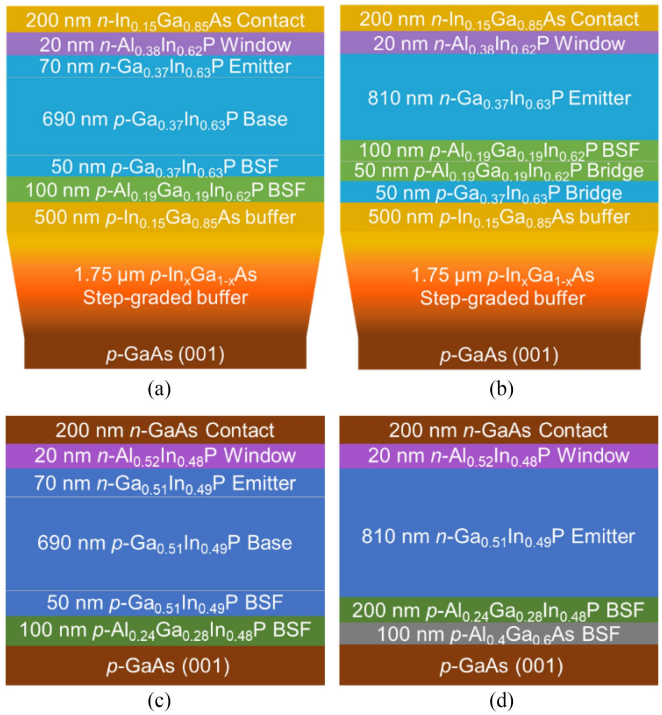

Fig. 1. Growth structures of (a) MM $Ga_{0.37}In_{0.63}P$ FJ, (b) MM $Ga_{0.37}In_{0.63}P$ RHJ, (c) LM $Ga_{0.51}In_{0.49}P$ FJ, and (d) LM $Ga_{0.51}In_{0.49}P$ RHJ solar cells.

III. Results and Discussion

A. Temperature-Dependent TRPL Lifetime Analysis

To investigate the dominant recombination mechanisms at high T, an analysis of T-dependent TRPL lifetime (τ_{TRPL}) was conducted on p- and n-GaInP DHs for both MM and LM cases. Taking into account different recombination lifetimes, including the radiative recombination lifetime (τ_r), Shockley–Read–Hall (SRH) recombination lifetime (τ_{SRH}) [23], interface recombination lifetime (τ_{int}), and recombination lifetime associated with thermionic emission (τ_{th}) [13], the effective carrier lifetime (τ_{eff}) can be represented as [12] follows:

$$\frac{1}{\tau_{eff}} = \frac{1}{\tau_r} + \frac{1}{\tau_{SRH}} + \frac{1}{\tau_{int}} + \frac{1}{\tau_{th}}.$$

This equation is applicable under low-injection conditions, where Auger recombination is negligible. The temperature

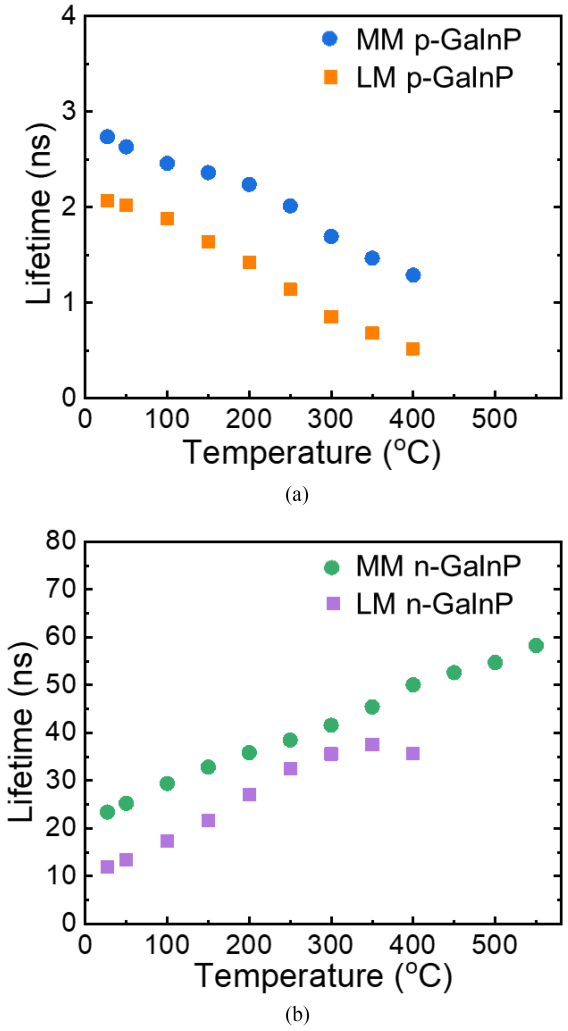

Fig. 2. TRPL lifetimes of (a) LM and MM p-GaInP DHs and (b) LM and MM n-GaInP DHs as a function of temperature.

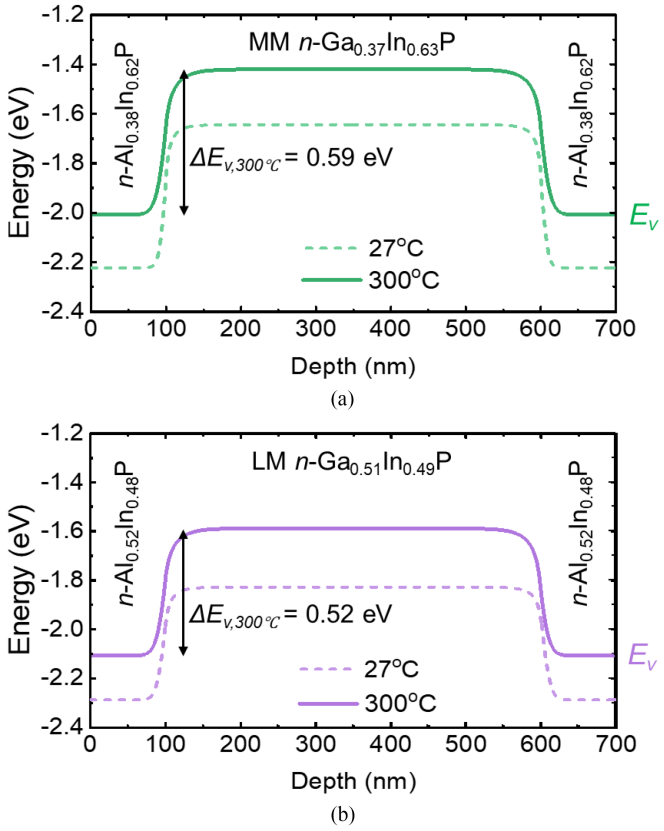

Fig. 3. Valence band diagrams of (a) MM n-GaInP DHs with MM n-$Al_{0.38}In_{0.62}P$ barriers and (b) LM n-GaInP DHs with LM n-$Al_{0.52}In_{0.48}P$ barriers at 27 °C (dashed lines) and 300 °C (solid lines), respectively. The diagrams depict only the valence bands and $\Delta E_{V,300\ °C}$ indicates the valence band offset at 300 °C.

dependencies of these lifetimes can be expressed as follows [24]:

$$\tau_r \propto T^{1.5},\ \tau_{\mathrm{SRH},}, \tau_{\mathrm{int},} \propto T^{-0.5}, \text{ and } \tau_{\mathrm{th}} \propto T^{-0.5} \cdot e^{\frac{\Delta E}{kT}}.$$

Note that τ_r increases weakly with T, τ_{SRH} decreases weakly with T, and τ_{th} decreases exponentially with T. By studying τ_{TRPL} as a function of T, the relative contributions of these recombination factors can be estimated at each specific T.

Fig. 2(a) shows that, as T increases to 400 °C, the τ_{TRPL} values for LM and MM p-GaInP decrease by ~4×, from 2.1 to 0.5 ns, and by ~2×, from 2.7 to 1.3 ns, respectively. The decrease in τ_{TRPL} suggests the dominance of SRH recombination, interface recombination, and/or thermionic emission [1] in both LM and MM p-GaInP. Specifically, a steep decline in τ_{TRPL}, signifying the onset of dominance of τ_{th} [12], [24], is observed above 100 °C for LM p-GaInP and above 200 °C for MM p-GaInP. The somewhat more gradual reduction in τ_{TRPL} for MM p-GaInP suggests a better suppression of thermionic emissions compared with LM p-GaInP [12], [25].

In contrast, both MM and LM n-GaInP exhibit an increase in τ_{TRPL} with increasing T, as shown in Fig. 2(b). The observed trend indicates the dominance of τ_r and the suppression of thermionic emission of minority holes in n-GaInP. For LM n-GaInP, τ_{TRPL} increases from 12 ns at RT before peaking at 37 ns at 350 °C, suggesting the dominance of thermionic emission effects over 350 °C. For MM n-GaInP, τ_{TRPL} starts from 23 ns at RT and rises to 58 ns at 550 °C; MM n-GaInP was the only sample that gave an adequate signal-to-noise ratio to extract the accurate lifetimes at such high T. The high τ_{TRPL} values in MM n-GaInP at such high T may stem from reduced thermionic emission owing to the higher valence band offset (ΔE_v) at the MM n-GaInP/MM n-AlInP interface (~0.58 eV at RT) compared with the LM n-GaInP/LM n-AlInP interface (~0.46 eV at RT), as illustrated by the calculated band diagrams in Fig. 3(a) and (b); at elevated T, the higher barrier heights in the MM are still maintained compared with LM, with ΔE_v values of 0.59 eV for MM and 0.52 eV for LM at 300 °C [solid lines in Fig. 3(a) and (b)]. The benefit of MM GaInP is further supported by the longer τ_{TRPL} values observed in both MM p- and n-GaInP compared with their LM counterparts, indicating longer τ_{SRH}, τ_{int}, and/or τ_{th} across the entire temperature range.

B. Advantages of MM Over LM GaInP FJ Cells at High T

In Fig. 4(a) and (b), IQE curves of LM and MM GaInP FJ cells show the expected shift to longer wavelengths due

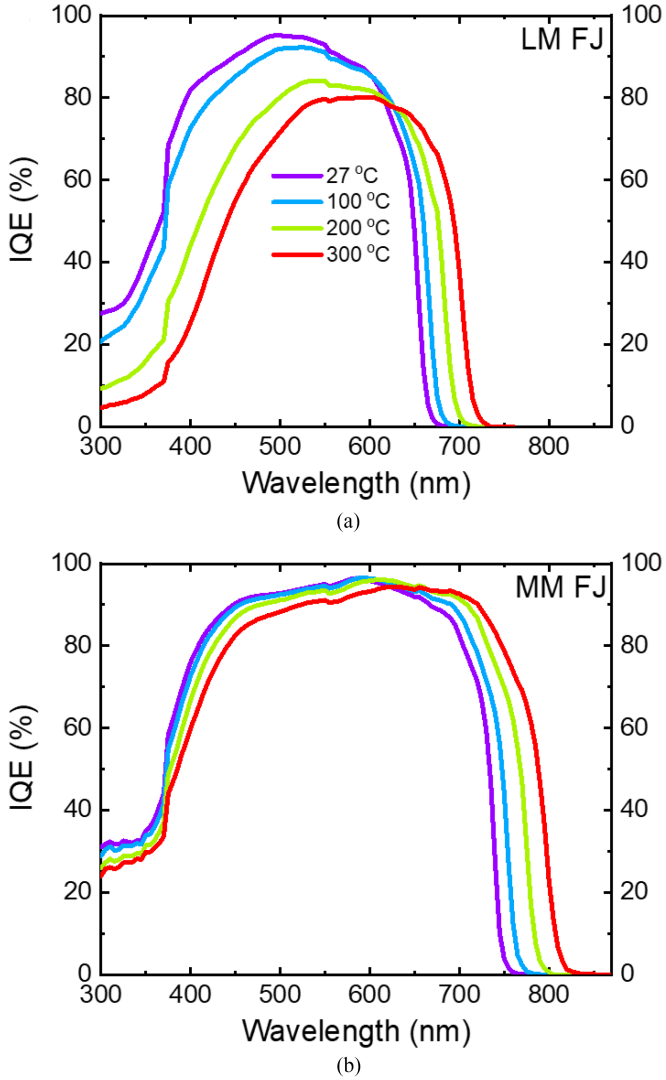

Fig. 4. IQE curves of (a) LM GaInP and (b) MM GaInP FJ cells at 27–300 °C.

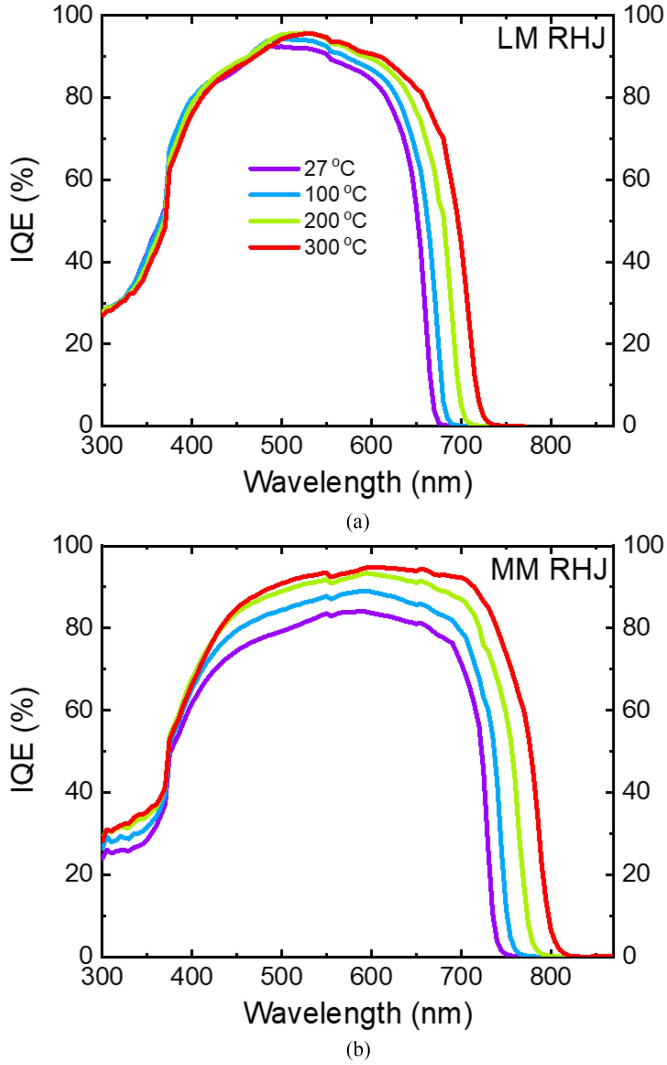

Fig. 5. IQE curves of (a) LM GaInP and (b) MM GaInP RHJ cells at 27–300 °C.

to E_g reduction as T increases. LM FJ cells undergo a slight drop in IQE as T increases to 100 °C, followed by a sharp decline at 100–300 °C [see Fig. 4(a)], consistent with the τ_{TRPL} trend observed in LM p-GaInP DHs. This steep decrease above 100 °C differs from what was reported by Perl [26] in metal-organic chemical vapour deposition (MOCVD)-grown LM GaInP FJ cells, where only a slight reduction in IQE at 300–550 nm occurred due to a decrease in E_g of the AlInP window. The discrepancy is likely due to the much shorter τ_{SRH} in our p-GaInP DHs compared with MOCVD-grown DHs (τ_{TRPL} ~29 and ~16 ns at RT and 300 °C, respectively) [12].

IQE of the MM FJ cells only experiences slight losses throughout visible wavelengths up to 300 °C that can be partially attributed to increased absorption in the window layer [see Fig. 4(b)]. The enhanced retention of IQE in MM FJ cells stems from the higher τ_{TRPL} and longer diffusion length of minority electrons in the MM p-GaInP base at high T compared with the LM p-GaInP base. Our MM FJ cells likely also benefit from a stronger suppression of thermionic emission due to the higher effective barrier height relative to LM FJ cells.

TABLE I
TEMPERATURE COEFFICIENTS OF LM AND MM GAINP CELLS WITH FJ AND RHJ CONFIGURATIONS

	$\frac{dV_{OC}}{dT}$ (mV/°C)	$\frac{dJ_{SC}}{dT}$ (mA/cm²·°C)	W_{OC} (V) @300°C
LM FJ	−2.55	−0.0022	1.070
LM RHJ	−2.46	+0.0078	0.999
MM FJ	−2.47	+0.0059	1.084
MM RHJ	−2.26	+0.0118	0.970

LM FJ cells show a negative value of $\frac{dJ_{SC}}{dT}$ due to a substantial decrease in peak IQE to ~80% at 300 °C (see Table I). On the other hand, the MM FJ cells demonstrate a slight increase in J_{SC} as T increases while maintaining a peak IQE of ~95%, showing the benefit of MM GaInP solar cells at high-T conditions. The slightly better $\frac{dV_{OC}}{dT}$ observed in MM FJ cells compared with LM FJ cells is also consistent with better τ_{TRPL} retention in MM cells at elevated T (see Table I).

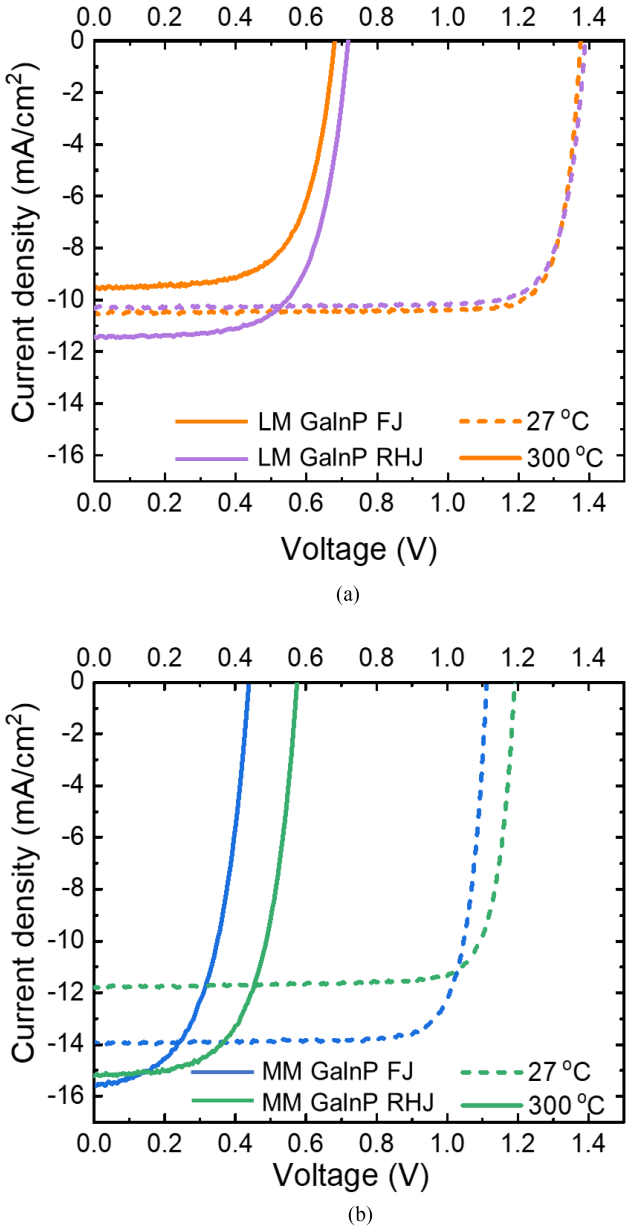

Fig. 6. LIV comparisons between (a) LM GaInP FJ and RHJ solar cells and (b) MM GaInP FJ and RHJ solar cells at 27 °C (dashed lines) and 300 °C (solid lines).

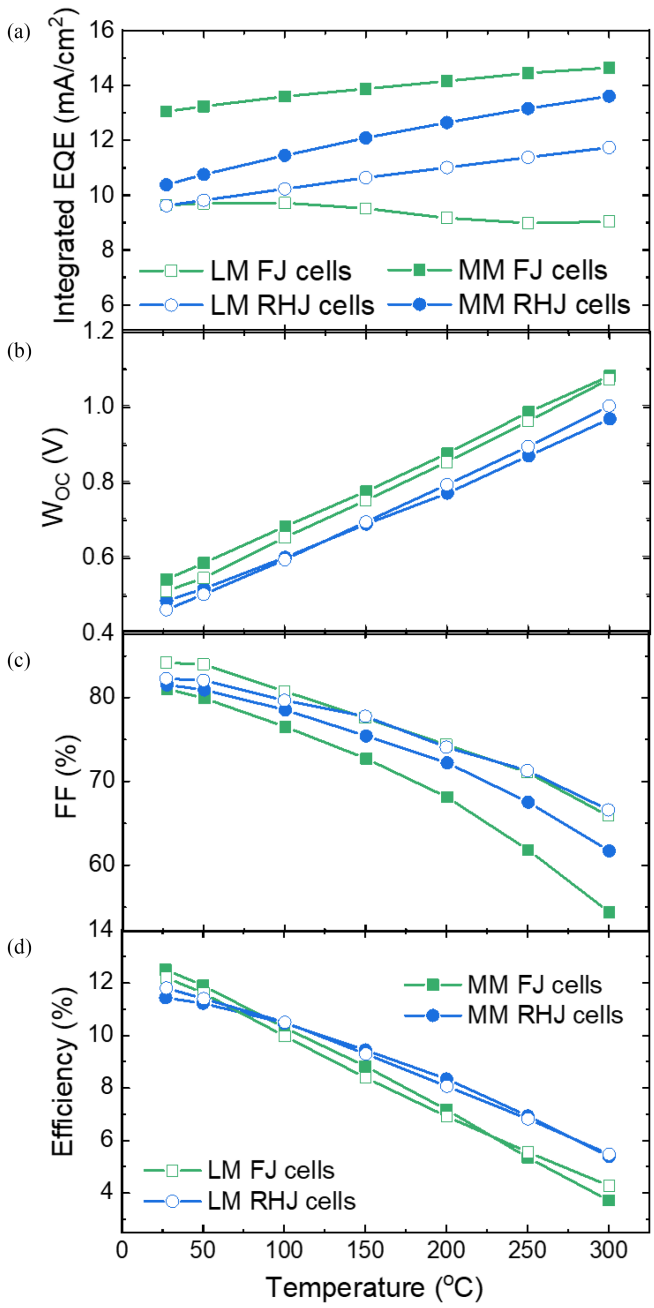

Fig. 7. (a) Integrated EQE, (b) W_{OC}, (c) FF, and (d) efficiency of MM and LM GaInP cells as a function of T. Filled and open symbols indicate MM and LM GaInP cells, respectively. Squares and circles indicate FJ and RHJ configurations, respectively.

C. *Advantages of RHJ Over FJ Cells at High* T

Fig. 5(a) and (b) demonstrates that IQE increases across all wavelengths up to 300 °C for both LM and MM RHJ cells due to the increase in τ_{TRPL} with T and the direct dependence of carrier diffusivity on T [27]. Between 27 and 300 °C, LM RHJ cells show a slight increase in peak IQE from ∼92% to ∼95%. In contrast, MM RHJ cells exhibit a strong boost in peak IQE from ∼84% to ∼95%, which can be attributed to the stronger increase in τ_{TRPL} in MM n-GaInP with T.

The LIV curves in Fig. 6(a) and (b) clearly show the advantages of RHJ cells over their FJ counterparts in terms of J_{SC}, V_{OC}, and FF at elevated T. While LM FJ and RHJ cells show similar V_{OC} and J_{SC} values at RT, LM RHJ cells display significantly higher V_{OC} and J_{SC} at 300 °C [see Fig. 6(a)]. The RHJ advantage is even more prominent for MM cells [see Fig. 6(b)]. Despite the lower J_{SC} at RT in MM RHJ cells, both MM FJ and RHJ cells exhibit similar J_{SC} values at 300 °C, while the V_{OC} advantage at 300 °C exceeds 110 mV [see Fig. 6(b)]. The enhanced V_{OC} retention in RHJ cells can be explained by lower dark current and thermionic loss of minority holes in n-GaInP. Table I further confirms the superior performance of RHJ cells at elevated temperatures, as evidenced by lower $\frac{dV_{OC}}{dT}$ and higher $\frac{dJ_{SC}}{dT}$ values compared with their FJ counterparts.

Notably, among all four configurations, MM RHJ cells show the lowest $\frac{dV_{OC}}{dT}$, the highest $\frac{dJ_{SC}}{dT}$, and the lowest W_{OC} value of 0.970 V at 300 °C (see Table I), benefiting from the advantages of both the higher barrier height and the RHJ configuration.

Fig. 7(a)–(d) summarizes all figures of merits, including integrated EQE, W_{OC}, FF, and efficiency for all four different solar cells as a function of T. Integrating EQE with the AM1.5G spectrum across all wavelengths [see Fig. 7(a)] reveals that the MM RHJ cell exhibits the strongest increase in J_{SC} with T. Fig. 7(b) shows a linear increase in W_{OC} with T for all cells due to the exponential increase in dark current. The advantage of RHJ cells (circles) over FJ cells (squares) in terms of W_{OC} becomes more prominent at higher T for both LM (open symbols) and MM (filled symbols) configurations. FF shows a qualitatively similar trend [see Fig. 7(c)], although the LM cells retain higher values than the MM cells due to their wider E_g. Furthermore, at RT, the RHJ cells have similar or lower FF values than FJ cells, whereas at 300 °C, higher FF is observed in RHJ cells compared with their FJ counterparts. The efficiency versus T plot in Fig. 7(d) captures all effects observed in Fig. 7(a)–(c) and demonstrates that the efficiency of the RHJ cells surpasses the FJ counterparts at $T > 100$ °C.

IV. Conclusion

In this article, we showed that the dark current advantage commonly observed in RHJ cells when compared with FJ cells persists at elevated T, enabling RHJ cells to outperform their FJ counterparts. While RHJ cells showed similar or poorer performance compared with FJ cells at RT, significant boosts in carrier collection from the long lifetime and thermally boosted diffusion length, as well as improved V_{OC} retention, were observed with increasing T. Taking advantage of the higher barrier height in MM GaInP, we found that the MM RHJ cells exhibited the lowest W_{OC} values among all the cells studied in this work at $T > 150$ °C, showing the beneficial effects of suppressing thermionic emission. Further investigations are necessary to develop low-resistance contacts with long-term stability.

Acknowledgment

This article made use of shared facilities in the Nick Holonyak, Jr. Micro and Nanotechnology Laboratory. The research was carried out in part at the Frederick Seitz Materials Research Laboratory Central Facilities, University of Illinois Urbana-Champaign.

References

[1] J. Simon, J. Geisz, D. Friedman, M. Steiner, and M. Lee, "Measurements and modeling of III-V solar cells at high temperatures up to 400 degrees C," *IEEE J. Photovolt.*, vol. 6, no. 5, pp. 1345–1352, Sep. 2016.

[2] R. Vaillon, S. Parola, C. Lamnatou, and D. Chemisana, "Solar cells operating under thermal stress," *Cell Rep. Phys. Sci.*, vol. 1, 2020, Art. no. 100267.

[3] J. Grandidier et al., "Low-intensity high-temperature (LIHT) solar cells for Venus atmosphere," *IEEE J. Photovolt.*, vol. 8, no. 6, pp. 1621–1626, Nov. 2018.

[4] J. Johny, S. Amos, and R. Prabhu, "Optical fibre-based sensors for oil and gas applications," *Sensors*, vol. 21, Sep. 2021, Art. no. 6047.

[5] S. Zhang and F. Yu, "Piezoelectric materials for high temperature sensors," *J. Amer. Ceram. Soc.*, vol. 94, pp. 3153–3170, 2011.

[6] H. Lee, V. Smet, and R. Tummala, "A review of SiC power module packaging technologies: Challenges, advances, and emerging issues," *IEEE J. Emerg. Sel. Topics Power Electron.*, vol. 8, no. 1, pp. 239–255, Mar. 2020.

[7] J. Watson and G. Castro, "A review of high-temperature electronics technology and applications," *J. Mater. Sci., Mater. Electron.*, vol. 26, pp. 9226–9235, 2015.

[8] E. E. Perl et al., "(Al)GaInP/GaAs tandem solar cells for power conversion at elevated temperature and high concentration," *IEEE J. Photovolt.*, vol. 8, no. 2, pp. 640–645, Mar. 2018.

[9] Y. Sun et al., "Thermal stability of GaAs solar cells for high temperature applications," in *Proc. IEEE 43rd Photovolt. Specialists Conf.*, 2016, pp. 2385–2388.

[10] M. A. Green, "General temperature dependence of solar cell performance and implications for device modelling," *Prog. Photovolt., Res. Appl.*, vol. 11, pp. 333–340, 2003.

[11] J. C. C. Fan, "Theoretical temperature dependence of solar cell parameters," *Sol. Cells*, vol. 17, pp. 309–315, 1986.

[12] E. E. Perl, D. Kuciauskas, J. Simon, D. J. Friedman, and M. A. Steiner, "Identification of the limiting factors for high-temperature GaAs, GaInP, and AlGaInP solar cells from device and carrier lifetime analysis," *J. Appl. Phys.*, vol. 122, 2017, Art. no. 233102.

[13] H. Schneider and K. V. Klitzing, "Thermionic emission and Gaussian transport of holes in a GaAs/$Al_xGa_{1-x}As$ multiple-quantum-well structure," *Phys. Rev. B*, vol. 38, pp. 6160–6165, 1988.

[14] J. F. Geisz, M. A. Steiner, I. Garcia, S. R. Kurtz, and D. J. Friedman, "Enhanced external radiative efficiency for 20.8% efficient single-junction GaInP solar cells," *Appl. Phys. Lett.*, vol. 103, Jul. 2013, Art. no. 041118.

[15] Y. Sun et al., "Improving the performance of GaInP solar cells through rapid thermal annealing and delta doping," *Sol. Energy Mater. Sol. Cells*, vol. 241, 2022, Art. no. 111725.

[16] Y. Sun, A. Perna, and P. Bermel, "Comparing front- and rear-junction GaInP photovoltaic devices through detailed numerical and analytical modeling," *IEEE J. Photovolt.*, vol. 9, no. 2, pp. 437–445, Mar. 2019.

[17] A. Abdollahi, M. M. Golzan, and K. Aghayar, "First-principles investigation of electronic properties of $Al_xIn_{1-x}P$ semiconductor alloy," *J. Mater. Sci.*, vol. 51, pp. 7343–7354, 2016.

[18] S. Ehsanfar, F. Kanjouri, H. Tashakori, and A. Esmailian, "First-principles study of structural, electronic, mechanical, thermal, and phonon properties of III-phosphides (BP, AlP, GaP, and InP)," *J. Electron. Mater.*, vol. 46, pp. 6214–6223, 2017.

[19] M. Kim, Y. Sun, R. D. Hool, and M. L. Lee, "Metamorphic front- and rear-junction 1.7 eV GaInP solar cells with high open-circuit voltage," *Sol. Energy Mater. Sol. Cells*, vol. 259, 2023, Art. no. 112435.

[20] Y. Sun et al., "Importance of long-lifetime n-GaInP for high-efficiency GaInP solar cells grown by MBE," in *Proc. IEEE 47th Photovolt. Specialists Conf.*, 2020, pp. 11–13.

[21] J. Faucher et al., "High-efficiency AlGaInP solar cells grown by molecular beam epitaxy," *Appl. Phys. Lett.*, vol. 109, 2016, Art. no. 172105.

[22] T. Masuda, S. Tomasulo, J. R. Lang, and M. L. Lee, "Comparison of single junction AlGaInP and GaInP solar cells grown by molecular beam epitaxy," *J. Appl. Phys.*, vol. 117, 2015, Art. no. 094504.

[23] Y. Rosenwaks, I. Tsimberova, H. Gero, and M. Molotskii, "Minority-carrier recombination in p-InP single crystals," *Phys. Rev. B*, vol. 68, 2003, Art. no. 115210.

[24] S. Liu et al., "Carrier lifetimes and interface recombination velocities in CdTe/$Mg_xCd_{1-x}Te$ double heterostructures with different Mg compositions grown by molecular beam epitaxy," *Appl. Phys. Lett.*, vol. 107, 2015, Art. no. 041120.

[25] F. J. Schultes et al., "Temperature dependence of diffusion length, lifetime and minority electron mobility in GaInP," *Appl. Phys. Lett.*, vol. 103, 2013, Art. no. 242106.

[26] E. Perl, "Material science for high-efficiency photovoltaics: From advanced optical coatings to cell design for high-temperature applications," Ph.D. dissertation, Dept. Elect. Comput. Eng., Univ. of California, Santa Barbara, CA, USA, 2016.

[27] X. Huang et al., "High-temperature polarization-free III-nitride solar cells with self-cooling effects," *ACS Photon.*, vol. 6, pp. 2096–2103, 2019.